Intersymbol Interference in Indoor Visible Light Communication Systems Employing LED Sources of Large Area

Marwa M. A. Elsaaty[a*], Adel Zaghloul[a], Khalid.F.A.Hussein[b]

a Electronics and Communications Engineering Dept., Zagazig University, Zagazig, Egypt
b Electronics Research Institute (ERI), Cairo, Egypt

A R T I C L E I N F O	A B S T R A C T
Keywords: Visible Light Communications, VLC, Inter-Symbol Interference. ISI.	This work is concerned with the assessment of inter-symbol interference (ISI) encountered in indoor visible light communication (VLC) system inside a room of relatively small dimensions (room area $\leq 5m \times 5m$). The signal-to-ISI ratio (SISIR) is evaluated over the horizontal plane of the mobile units (at a height of about 1m above the room floor). The present paper provides performance assessment of the VLC system employing a light source of wide rectangular area in comparison to the VLC system employing a point LED source. It is assumed that the indoor light propagation is impaired by noise including ambient light, shot noise and thermal noise. The overall noise is modelled as additive white Gaussian noise (AWGN). The signal-to-interference-plus-noise ratio (SINR) including the effects of ISI and AWGN is evaluated over the horizontal plane of the mobile units. The corresponding bit-error-rate (BER) is also evaluated. The dependencies of the average propagation delay, root-mean-squared (RMS) delay spread, and SINR on the area of the LED source are numerically investigated. It is shown the SISIR for the indoor VLC system under consideration is significantly decreased with increasing the area of the LED source. Also, it is shown that the performance of the VLC is degraded with increasing the area of the LED source. The effect of increasing the radiated light power is shown to decrease the BER error rate and, hence, to improve the VLC performance especially at the room corners.

1. Introduction

Most of the currently operational wireless communication systems are employing the radio frequency (RF) and microwave spectra. As a consequence of the rapidly increasing population of mobile communication users, the wireless communications face a serious shortage regarding spectrum allocation. The visible light communication (VLC) systems utilize the wide spectrum of visible light for wireless communications [1-14]. The visible light spectrum is capable of offering much higher

transmission rates than those offered by microwave spectrum. Moreover, the VLC systems are more immune to electromagnetic interference than the immunity of the microwave wireless communication systems. Also, the VLC systems have the advantage of using the general lighting sources such as the light-emitting diode (LED) through high-speed on/off switching to transmit data at high rates. Photosensitive components such as photodetectors can be used to receive the signals sent by the lighting sources. Thus, the VLC enables the efficient use of the simple on/off keying (OOK) modulation as a

digital intensity modulation technique for high data rate transmission with high noise immunity.

In indoor VLC system, the light source should meet the requirement for room lighting in addition to signal coverage. This requires the installation of LED source with appropriate shape and distribution. For a room of, relatively, small area ($\leq 5m \times 5m$) the lighting may be performed by employing a single point LED source mounted at the center of the room ceil; see Figure 1a. For more uniform illumination, the light source can be constructed as an array of small LED sources and may have a rectangular area that is large enough to produce more uniform illumination than that produced by a single (point) source; see Figure 1b.
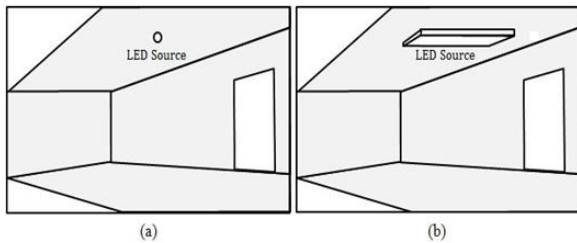
Fig.1: Two types of LED sources used for indoor VLC in the present study. (a) Point LED source. (b) LED source of rectangular area.

The present work may be considered as providing a comparative study between the performance of the VLC system employing a point LED source and that of the VLC system employing a light source of rectangular area. For the comparison to be objective, it is assumed that the light power radiated from the point LED source is the same as the power radiated from the rectangular LED source irrespective of its area.

In the present study, it is assumed that the responsivity of the photodetector is unity, and the field-of-view (FOV) is $90°$. The sidewalls of the room are assumed to be Lambertian reflective surfaces with unity Lambert index.

The present work provides a complete description of the method used to evaluate the inter-symbol interference (ISI) in the plane of the mobile receivers for both types of LED sources. In the case of a point LED source, the ISI results only from the reflection of light on the side walls of the room, i.e. from the non-line-of-sight (non-LOS) propagation. However, in the case of a square LED source, the ISI results from LOS and non-LOS propagation.

As regarding the environmental effects, the light propagation impairments of optical communication channels are dominated by ambient-induced shot-noise that can be modeled as a Gaussian process

[8,14]. In the present analysis, it is assumed that the indoor light propagation is impaired by noise including ambient light, shot noise and thermal noise. The overall noise can be modelled as additive white Gaussian noise (AWGN). In the present work, the signal-to-interference-plus-noise ratio (SINR) including the effects of ISI and AWGN is evaluated over the horizontal plane of the mobile units. The corresponding distribution of the bit-error-rate (BER) over the same area is evaluated assuming that the on-off keying modulation technique is employed.

It may be worthwhile to mention that, in addition to the new mathematical model developed for the assessment of the intersymbol interference through the calculation of the reflections of the light rays on the room walls, one of the novelty aspects of the present paper is its main contribution which is represented by the application of the Geometrical Theory of Diffraction in conjunction with the Ray-Tracing (GTD-RT) method described in references [16, 17] to evaluate the reflection of the light waves on the room wall instead of using the approximate Lambertian cosine Law found in most of the literature. This requires modelling the room walls as rough surfaces using the Savitzky-Golay method as described in reference [18].

2. Indoor VLC Channel Model

It is assumed that the room is empty and has its interior of a cuboidal shape whose dimensions are W_x, W_y, and W_z in the x-, y-, and z-directions, respectively. The LED source is assumed to be Lambertian radiator with unity Lambert index and is mounted on the room ceil with the maximum luminous intensity directed normal to the room ceil in the downward direction. On the other hand, the mobile, or even stationary, receivers are assumed as photodetectors that can freely move in the horizontal plane at a height of z_r above the room floor.

In the present study, the side walls of the room are assumed to be optically rough and, hence, the reflection of the light on these walls depends on the wall roughness and can be accurately evaluated using the method described in [15-17]. However, for the present study it may be accurate enough to assume that the side walls have Lambertian reflective surfaces (reflectance > 0) with unity Lambert index. As the present study focuses only on the channel (propagation) model, the photodetector responsivity is assumed to be unity; $\eta = 1$. Also, the FOV of the receiving photodetector is assumed to be $90°$.

In this way, a point in the plane of the receiver units can be illuminated from the following sources:

1. Direct illumination (LOS) from the LED source(s).
2. Indirect illumination (non-LOS) due to the reflection of the light on the sidewalls of the room.
3. Noise resulting from ambient light of the sun, fluorescent lambs, or any other unplanned source.

2.1. Impulse Response for Point Light Source

In this section, it is assumed that a small LED source is used for VLC in the room as shown in Figure 1a. This light source is located at the center of the room ceil as shown in Figure 2 and can be considered a point source. The luminous flux intensity $I(\theta)$ due to a point LED source mounted in the room ceil is the direction making angle θ with the normal to the ceil (see Figure 2) is defined as the luminous flux within the unit solid angle at this direction.

$$I_a(\theta) = (d\Phi(\theta))/d\Omega \tag{1}$$

Where $d\Phi(\theta)$ is the luminous flux within the solid angle $d\Omega$ in the direction θ.

The radiation from the point LED source located at the center of the room ceil, as shown in Figure 2, can be described by the spatial angular distribution of the luminous flux intensity $I_a(\theta)$, which is assumed to be Lambertian.
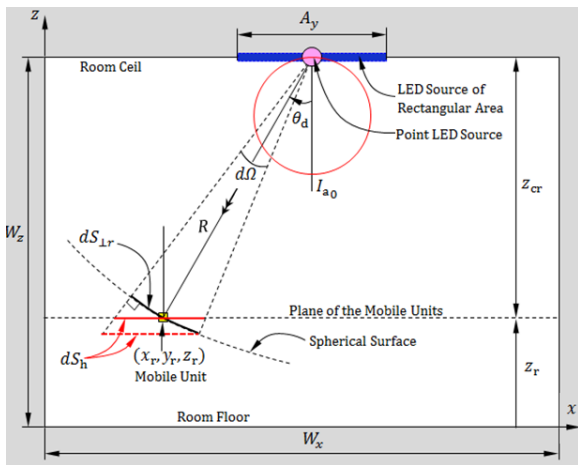
Fig.2: Light wave propagation model for calculation of the direct (LOS) horizontal illuminance at the location of the mobile unit

$$I_a(\theta) = I_{a_0} \cos\theta \tag{2}$$

2.1.1. Direct (LOS) Illuminance from Point Light Source

The illuminance of a surface segment $dS_{\perp r}$ at the location of a receiver at $\mathbf{r_r} \equiv (x_r, y_r, z_r)$, (shown in Figure 2) of a sphere whose center is at the point LED source can be expressed as follows.

$$E_{S_{\perp r}} = \frac{d\Phi}{dS_{\perp r}} = \frac{I_a(\theta_d)d\Omega}{dS_{\perp r}} \tag{3}$$

Where $d\Omega$ is the solid angle subtending the area $dS_{\perp r}$ that is given as

$$dS_{\perp r} = R^2 d\Omega \tag{4}$$

Where R is the distance between the LED source and the mobile receiver.

By substitution from (4) into (3), one gets the following expression

$$E_{S_{\perp r}} = \frac{I_a(\theta_d)}{R^2} = \frac{I_{a_0}\cos\theta_d}{R^2} \tag{5}$$

The illuminance of the horizontal surface at $\mathbf{r_r}$ can be expressed as follows.

$$E_d = E_{S_{\perp r}}\cos\theta_d = \frac{I_{a_0}\cos^2\theta_d}{R^2} \tag{6}$$

The distance, R, between the LED source and the mobile receiver can be expressed in terms of the ceil height, z_{cr}, relative to the plane of the mobile receivers as follows.

$$R = |\mathbf{r_r} - \mathbf{r_c}| = \frac{z_{cr}}{\cos\theta_d} \tag{7}$$

where $\mathbf{r_c} = (W_x/2, W_y/2, W_z)$ is the position vector of the center point of the room ceil.

The Substitution from (7) into (6) results in the following expression for the horizontal illuminance in the plane of the mobile receivers due to a point LED source.

$$E_d \equiv E(\theta_d) = \frac{I_{a_0}\cos^4\theta_d}{z_{cr}^2} \tag{8}$$

The total luminous flux is equal to the total light power, P_{Tx}, radiated from the from the LED source. Hence,

$$P_{Tx} = \int_{\text{half space}} d\Phi = \int_{\text{half space}} I_a(\theta) \, d\Omega \qquad (9)$$

Considering that $d\Omega = \sin\theta \, d\theta \, d\phi$, the last integral can be expressed as follows.

$$P_{Tx} = \int_0^{2\pi} \int_0^{\pi/2} I_{a_0} \cos\theta \, \sin\theta \, d\theta \, d\phi \qquad (10)$$

Thus,

$$P_{Tx} = I_{a_0} \int_0^{2\pi} d\phi \int_0^{\pi/2} \frac{1}{2}\sin(2\theta) \, d\theta \qquad (11)$$

Thus, the maximum luminous flux intensity, I_{a_0}, of the LED source can be expressed in terms of the transmitted optical power, P_{Tx}, as follows.

$$I_{a_0} = \frac{P_{Tx}}{\pi} \qquad (12)$$

The impulse response due to a point LED source can be expressed as follows

$$h_d(t) = \frac{P_{Tx} \cos^4\theta_d}{\pi z_{cr}^2} \, \delta(t - t_a) \qquad (13)$$

where t_a is the time taken by an optical impulse to travel from the point LED source at $\mathbf{r}_c$ to the receiver at $\mathbf{r}_c$.

$$t_a = \frac{1}{c_0}|\mathbf{r}_r - \mathbf{r}_c| = \frac{z_{cr}}{c_0 \cos\theta_d} \qquad (14)$$

where c_0 is the speed of light in free space.

2.1.2. Indirect (Non-LOS) Illuminance from Point Light Source

Referring to Figure 3, the illuminance of the side wall $x = 0$, at a point $\mathbf{r}_w \equiv (0, y_w, z_w)$ can be expressed as follows.

$$[E_w]_{\mathbf{r}_w} = \left[\frac{I_a(\theta_a)}{R_{wa}^2} \cos\theta_{wa}\right]_{\mathbf{r}_w} \\ = I_{a_0}\left[\frac{\cos\theta_a \cos\theta_{wa}}{R_{wa}^2}\right]_{\mathbf{r}_w} \qquad (15)$$
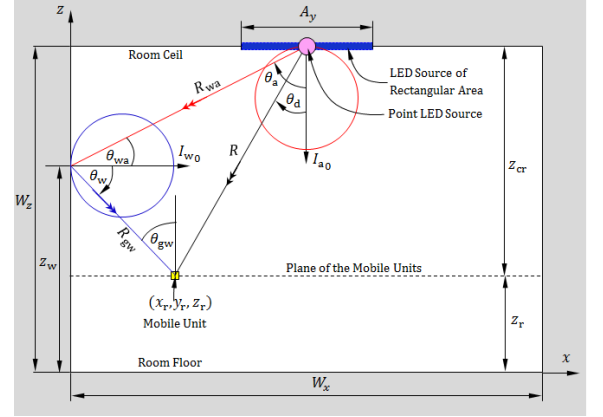
Fig.3: Light wave propagation model for calculation of indirect (non-LOS) horizontal illuminance at the location of the mobile unit.

The power (luminous flux) of the light emitted from the wall segment $dy_w \, dz_w$ at the point $\mathbf{r}_w$ can be expressed as follows.

$$[\Phi_w]_{\mathbf{r}_w} = [G_w E_w]_{\mathbf{r}_w} \, dx_w \, dz_w \qquad (16)$$

Where G_w is the wall reflectance at the point $\mathbf{r}_w$.
The wall segment $dy_w \, dz_w$ at the point $\mathbf{r}_w$ can be considered as a secondary radiator. As the wall is assumed as a Lambertian rough surface, the luminous flux intensity of the light emitted from this wall segment can be expressed as follows.

$$[I_w(\theta_w)]_{\mathbf{r}_w} = \left[I_{w_0} \cos\theta_w\right]_{\mathbf{r}_w} \qquad (17)$$

where $\left[I_{w_0}\right]_{\mathbf{r}_w}$ is the luminous flux intensity in the direction normal to the wall due to the emission from the wall segment $dy_w \, dz_w$ at the point $\mathbf{r}_w$.
Also, the luminance intensity of the light reflected from the wall segment $dy_w \, dz_w$ in the direction of the mobile unit at $\mathbf{r}_r$ can be expressed as follows.

$$[I_w(\theta_w)]_{\mathbf{r}_w} = \left[\frac{d\Phi_w}{d\Omega}\right]_{\mathbf{r}_w} \qquad (18)$$

Thus, the total luminous flux Φ_w emitted from the wall segment $dy_w \, dz_w$ at $\mathbf{r}_w$ can be obtained as follows.

$$[\Phi_w]_{\mathbf{r}_w} = \int_{\text{half space}} [I_w(\theta)]_{\mathbf{r}_w} \, d\Omega \qquad (19)$$

Considering that $d\Omega = \sin\theta \, d\theta \, d\phi$, the last integral can be expressed as follows.

$$[\Phi_w]_{r_w} = \int_0^{2\pi} \int_0^{\pi/2} [I_{w_0}]_{r_w} \cos\theta \sin\theta \, d\theta \, d\phi \qquad (20)$$

Thus,

$$[\Phi_w]_{r_w} = [I_{w_0}]_{r_w} \int_0^{2\pi} d\phi \int_0^{\pi/2} \frac{1}{2}\sin(2\theta) \, d\theta \qquad (21)$$

Thus, the total luminous flux $[\Phi_w]_{r_w}$ emitted from the wall segment $dy_w \, dz_w$ at the point r_w can be expressed in terms of the maximum luminous flux intensity, $[I_{w_0}]_{r_w}$, as follows.

$$[\Phi_w]_{r_w} = \pi [I_{w_0}]_{r_w} \qquad (22)$$

Making use of (15), (16), and (22), the maximum luminous flux intensity, $[I_{w_0}]_{r_w}$, can be expressed as follows.

$$[I_{w_0}]_{r_w} = \frac{I_{a_0}}{\pi} \left[G_w \frac{\cos\theta_a \cos\theta_{wa}}{R_{wa}^2} \right]_{r_w} dx_w \, dz_w \qquad (23)$$

The horizontal illuminance at the photodetector of the mobile receiver due to the indirect radiation from the wall segment $dy_w \, dz_w$ at r_w can be expressed as follows.

$$[dE_i]_{r_w} = \left[\frac{I_{w_0} \cos\theta_w \, \cos\theta_{gw}}{R_{gw}^2} \right]_{r_w} \qquad (24)$$

By substitution from (23) into (24), the following expression is obtained.

$$[dE_i]_{r_w} = [\xi_i]_{r_w} \, dx \, dz \qquad (25)$$

where,

$$[\xi_i]_{r_w} = \frac{P_{Tx}}{\pi^2} \left[G_w \frac{\cos\theta_a \cos\theta_{wa} \cos\theta_w \, \cos\theta_{gw}}{R_{wa}^2 \, R_{gw}^2} \right]_{r_w} \qquad (26)$$

The component of the non-LOS impulse response due to the reflection of light on the wall #1 ($x = 0$) can be expressed as follows.

$$[h_i(t)]_1 = \int_{z_r}^{W_z} \int_0^{W_y} [\xi_i]_{r_w} \, \delta(t - t_w) \, dy_w \, dz_w \qquad (27)$$

where t_w is the total time taken by an optical impulse when it is transmitted by the point LED source, then reflected on the surface segment at r_w (on the wall $y = 0$) and, finally, arrives at the location of the receiver r_r.

$$t_w = \frac{1}{c_0} \left(|r_w - r_c| + |r_r - r_w| \right) \qquad (28)$$

The total non-LOS impulse response at the mobile receiver can be obtained by performing the integration expressed in (27) on each of the four side walls of the room and then summing the integral values as follows.

$$h_i(t) = \sum_{q=1}^4 [h_i(t)]_q \qquad (29)$$

Considering that the mobile receiver has its FOV $\leq$ 90°, the area of the side wall #1($x = 0$) subtended between the planes $z = z_r$ and $z = W_z$ can be discretized with fine enough resolution to a number of rectangular segments of equal area $\Delta s = \Delta y \Delta z$. The illuminance at the location of the receiver due to the light reflected from the wall segment number m, n can be expressed as follows.

$$[\Delta E_{i_{m,n}}]_1 = [\Delta s \xi_{i_{m,n}}]_1, \qquad \begin{array}{l} m = 1,2,..,M_1, \\ n = 1,2,..,N_1 \end{array} \qquad (30)$$

where M_1 and N_1 are the number of segments which the side wall #1 is discretized in the vertical and horizontal directions, respectively, and $\xi_{i_{m,n}}$ is given as follows.

$$[\xi_{i_{m,n}}]_1 = [\xi_i]_{r_w=[0,(m-1)\Delta y,(n-1)\Delta z]} \qquad (31)$$

The total (indirect) impulse response due to the light reflection on the four side walls is the horizontal illuminance due to the light arriving at the receiver location through non-LOS propagation and can be expressed as follows.

$$h_i(t) = \sum_{q=1}^4 \sum_{m=1}^{M_q} \sum_{n=1}^{N_q} [\Delta E_{i_{m,n}}]_q \, \delta(t - t_{q,m,n}) \qquad (32)$$

where M_q and N_q are the number of segments to which the qth side wall is discretized in the vertical and horizontal directions, respectively; $t_{q,m,n}$ is the total time taken by an optical impulse when it is

transmitted by the point LED source at $t = 0$, then reflected on the surface segment number m, n on the qth side wall, and finally arrives at the location of the receiver $\mathbf{r_r}$.

$$t_{m,n} = \frac{1}{c_0} \left[R_{\text{wa}} + R_{\text{gw}} \right]_{m,n} \tag{33}$$

2.2. Impulse Response for Light Source of Rectangular Area

In this section it is assumed that the light source used for VLC in the room is planar and has a rectangular area $A_x A_y$ and located at the center of the room ceil as shown in Figure 1b. It is assumed that the total light power, $\boldsymbol{P_{Tx}}$, (luminous flux) radiated from the LED source of rectangular area is the same as that radiated from the point LED source considered in Section 2.1. The radiation from an area segment $dx_a dy_a$ at the location $\mathbf{r_a} \equiv (x_a, y_a, W_z)$ on this rectangular LED source, can be described by the spatial angular distribution of the luminous flux intensity $d\boldsymbol{I_a(\theta)}$, which is assumed to be Lambertian.

$$\left[dI_a(\theta) \right]_{\mathbf{r_a}} = I_{a0} \frac{dx_a dy_a}{A_x A_y} \frac{z_{\text{cr}}}{R_{\text{ra}}} \tag{34}$$

Where $\boldsymbol{R_{ra}} = |\mathbf{r_r} - \mathbf{r_a}|$.

2.2.1. Direct (LOS) Illuminance from Light Source of Rectangular Area

The horizontal illuminance in the plane of the mobile receivers due to the light emitted from an area segment $dx_a dy_a$ at $\mathbf{r_a}$ on this rectangular LED source can be expressed as follows.

$$\left[dE_d \right]_{\mathbf{r_a}} = \frac{P_{Tx}}{\pi^2} \frac{dx_a dy_a}{A_x A_y} \frac{z_{\text{cr}}^2}{R_{\text{ra}}^4} \tag{35}$$

The impulse response at $\mathbf{r_r}$ can be obtained by integrating (35) over the source area as follows.

$$h_d(t) = \frac{P_{Tx} z_{\text{cr}}^2}{\pi^2 A_x A_y} \int_{-A_y/2}^{-A_y/2} \int_{-A_x/2}^{A_x/2} \frac{1}{R_{\text{ra}}^4} \delta(t - t_a) \, dx_a \, dy_a \tag{36}$$

Where, $\boldsymbol{R_{ra}} = |\mathbf{r_r} - \mathbf{r_a}|$ and $\boldsymbol{t_a}$ is the time taken by an optical impulse to arrive at the receiver through the LOS when it is emitted from the source segment

$dx_a dy_a$ at the location $\mathbf{r_a}$ on the rectangular LED source.

$$t_a = \frac{1}{c_0} |\mathbf{r_r} - \mathbf{r_a}| \tag{37}$$

2.2.2. Indirect (Non-LOS) Illuminance from Light Source of Rectangular Area

The indirect horizontal illuminance at the receiver due to the light impulse originally radiated from source segment $dx_a dy_a$ at $\mathbf{r_a}$ on the rectangular LED source and then reflected on the wall segment $dx_w dz_w$ at $\mathbf{r_w}$ can be expressed as follows.

$$\left[dE_i \right]_{\mathbf{r_w}, \mathbf{r_a}} = \left[d\xi_i \right]_{\mathbf{r_w}, \mathbf{r_a}} dx_w dz_w \tag{38}$$

where,

$$[d\xi_i]_{\mathbf{r_w}, \mathbf{r_a}}$$
$$= \frac{P_{Tx}}{\pi^2 z_{\text{cr}}^2} \frac{dx_a dy_a}{A_x A_y} \left[\frac{G_w \cos \theta_a \cos \theta_{wa} \cos \theta_w \ \cos \theta_{gw}}{R_{\text{wa}}^2 \ R_{\text{gw}}^2} \right]_{\mathbf{r_w}, \mathbf{r_a}} \tag{39}$$

The non-LOS impulse response at the mobile receiver $\mathbf{r_r}$ can be obtained by, first, integrating the quantity given by (38) on each side wall and on the area of the rectangular LED source; for example the non-LOS impulse response due to the side wall #1 $(x = 0)$ can be expressed as follows.

$$[h_i(t)]_1$$
$$= \frac{P_{Tx}}{\pi^2 z_{\text{cr}}^2 A_x A_y} \int_0^{A_y} \int_0^{A_x} \int_{z_r}^{W_z} \int_0^{W_y} [d\xi_i]_{\mathbf{r_w}, \mathbf{r_a}} \, \delta(t - t_{w,a}) \ dy_w \ dz_w \, dx_a \, dy_a \tag{40}$$

where $t_{w,a}$ is the time taken by a light impulse that is emitted from the source segment $dx_a dy_a$ at $\mathbf{r_a}$ on the rectangular LED source, to arrive at the receiver $\mathbf{r_r}$ through the reflection on the wall segment $dx_w dz_w$ at $\mathbf{r_w}$.

$$t_{w,a} = \frac{1}{c_0} \left(|\mathbf{r_w} - \mathbf{r_a}| + |\mathbf{r_r} - \mathbf{r_w}| \right) \tag{41}$$

The integral expressed in (40) is calculated for each side wall and, then, the total non-LOS impulse response is obtained by carrying out the following summation.

$$h_i(\text{t}) = \sum_{q=1}^{4} [h_i(\text{t})]_q \qquad (42)$$

where q is an index for the side walls

2.3. Modeling Noise and Ambient Light in VLC systems

It is well known that the light propagation impairments of optical communication channels are dominated by ambient-induced shot-noise that can be modeled as a Gaussian process [14]. In the present analysis, it is assumed that the indoor light propagation is impaired by noise including ambient, shot noise and thermal noise. The overall noise can be modeled as AWGN. It is, also, assumed that the OOK modulation technique is employed in the indoor VLC system where the transmitted pulse can be considered as a rectangular pulse of duration equal to the bit period, $T_b = 1/R_b$. Upon the knowledge of the total impulse response, $h(t)$, the received pulse can be expressed as follows.

$$x_r(t) = s_r(t) + n(t) \qquad (43)$$

where $n(t)$ represents the instantaneous value added to the signal at the receiver due to the noise (including ambient noise, shot noise, and thermal noise). The noise represented by $n(t)$ can be modeled as AWGN [8, 14]. The term $s_r(t)$ denotes the signal received due to the impulse response of the indoor VLC propagation channel; it can be expressed as follows.

$$s_r(t) = \eta \, s_t(t) \otimes h(t) \qquad (44)$$

Where η is the responsivity of the receiving photodetector. In the present study, the photodetector responsivity is assumed to be unity; $\eta = 1$.

2.4. Assessment of Root-Mean-Squared Propagation Delay

In indoor VLC systems, the received optical pulse is subjected to delay spread due to multipath propagation. The transmitted optical pulse representing a bit in the OOK modulation system travels in different paths with variable lengths and, hence, arrives at the position of the receiver at varying times, which causes the received pulse representing a bit to be spread and overlapped with the subsequent bits. The RMS delay spread is a measure of the ISI caused by multipath channel of the indoor propagation.

The average propagation delay, T_{av}, can be calculated once the impulse response $h(t)$ is obtained using the following integral.

$$T_{av} = \frac{\int_{-\infty}^{\infty} t \, h^2(t) \, dt}{\int_{-\infty}^{\infty} h^2(t) \, dt} \qquad (45)$$

The RMS propagation delay, T_{rms}, can be evaluated as follows.

$$T_{av} = \frac{\int_{-\infty}^{\infty} (t - T_{av})^2 \, h^2(t) \, dt}{\int_{-\infty}^{\infty} h^2(t) \, dt} \qquad (46)$$

The integrals (45) and (46) can be numerically evaluated once the impulse response $h(t)$ is determined.

2.5. Assessment of Power of Intersymbol Interference

Let us introduce the reference pulse, which is useful for evaluating the distortion of the received pulse and the calculation of the ISI. The reference pulse can expressed as follows.

$$s_{REF}(t) = s_t(t) \otimes h_d(t) \qquad (47)$$

Where $s_t(t)$ is the transmitted pulse $h_d(t)$ is given by (13). This definition means that the reference pulse is the subjected to the time shift equal to the propagation delay through the LOS and subjected to amplitude decay equal to the spread loss of the light intensity as it propagates from the transmitter to the receiver.

The SISIR is the ratio between the light energy of the received pulse to the energy interfering the other pulses due to the delay spread of the received pulse. The signal energy, E_S, is the energy received within the duration of the reference pulse and can be evaluated as follows.

$$E_S = \int_{t_a}^{t_a + T_b} s_r(t) dt \qquad (48)$$

Where t_a is the time of arrival of the received pulse (the start time of the reference pulse)

The ISI is the energy received after the end time of the reference pulse and, hence, it can be calculated as follows

$$E_{ISI} = \int_{t_a+T_b}^{\infty} s_r(t)\, dt \qquad (49)$$

Thus, the SINR regarding the ISI can be expressed as follows.

$$SISIR = \frac{E_S}{E_{ISI}} = \frac{\int_{t_a}^{t_a+T_b} s_r(t)\, dt}{\int_{t_a+T_b}^{\infty} s_r(t)\, dt} \qquad (50)$$

The assessment of the SINR due to ISI only can be evaluated by numerical evaluation of the integrals in (50).

3. Results and Discussions

It should be noted that throughout all of the following presentations and discussions the total light power radiated from the point LED sources is equal to the power radiated from the LED source of rectangular area and both are set to $P_{Tx} = 10\,W$ unless otherwise indicated.

3.1. ISI at Arbitrary Point in Indoor VLC System

Consider the case shown in Figure 4 for a mobile unit (receiver) at the point $\mathbf{r} = (\mathbf{1m}, \mathbf{2m}, \mathbf{1m})$. Two types of LED sources are considered; the first type is a point LED source and the other type is a square LED source of area $\mathbf{45\,cm \times 45\,cm}$. The present section is concerned with the investigation of the impulse response at the location of the indicated receiver due to both types of LED sources.
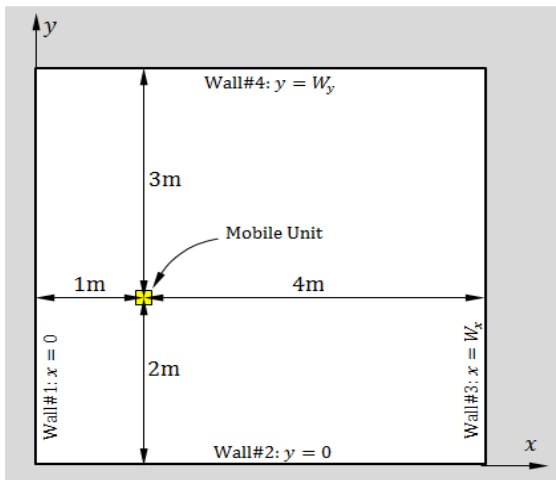
Fig.4: Location of the receiving unit, r = (1m, 2m, 1m) inside a room of dimensions 5m × 5m × 3m.

3.1.1. Impulse Response at Arbitrary Point

The impulse response at the location $\mathbf{r} = (\mathbf{1m}, \mathbf{2m}, \mathbf{1m})$ is presented in Figure 5. As shown in Figure 5a, the LOS impulse response is a Dirac-delta function $\boldsymbol{\delta(t - t_a)}$, $\boldsymbol{t_a = 8.6\,ns}$, which is the time of arrival of the light impulse transmitted by a point LED source at the center of the ceil room. The non-LOS impulse response is shown in Figure 5b. Each of the four peaks of the impulse response is caused by the light reflection on one of the four side walls of the room. The first peak is the highest one and is caused by light impulse reflection

On the nearest wall to the receiver ($\boldsymbol{x = 0}$). The fourth peak is the lowest one and is caused by light reflection on the farthest wall ($\boldsymbol{x = W_x}$).
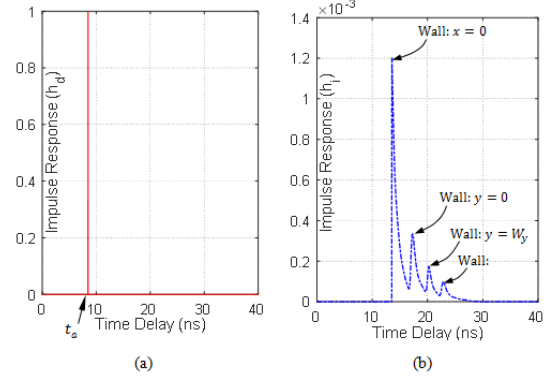
Fig.5: Normalized impulse response at a point r = (1m, 2m, 1m) inside a room of dimensions 5m × 5m × 3m due a point LED source mounted at the center point of the room ceil , (a) LOS impulse response. (b) Non-LOS impulse response.

The impulse response at the same location of the receiver, due to a square LED source of area (45cm × 45cm), is presented in Figure 6. The normalized LOS impulse response is a narrow pulse of non-zero width as shown in Figure 6a. The non-LOS impulse response is a spread pulse with four peaks as shown in Figure 6b. The first peak is the highest one and is caused by light impulse reflection on the nearest wall to the receiver ($x = 0$). The fourth peak is the lowest one and is caused by light reflection on the farthest wall ($x = W_x$).

The total impulse response at the location $\mathbf{r} = (\mathbf{1m}, \mathbf{2m}, \mathbf{1m})$ due to a point LED source is shown in Figure 7a. As the level of magnitude of the non-LOS response is very low relative to that of the LOS response, log scale is used for the vertical axis to show both responses together. As shown in this figure, the total impulse response has two distinct components; one is a Dirac-delta function, whereas

the other component has a duration over the interval $(13 - 30 \text{ ns})$ of the delay time. The total impulse response at the location $\mathbf{r} = (1\text{m}, 2\text{m}, 1\text{m})$ due to a square LED source of area $45 \text{ cm} \times 45 \text{ cm}$ is shown in Figure 7b. It is shown that the relative magnitude of the non-LOS to the LOS component of the impulse response for the square LED source is much larger than that for the point LED source.
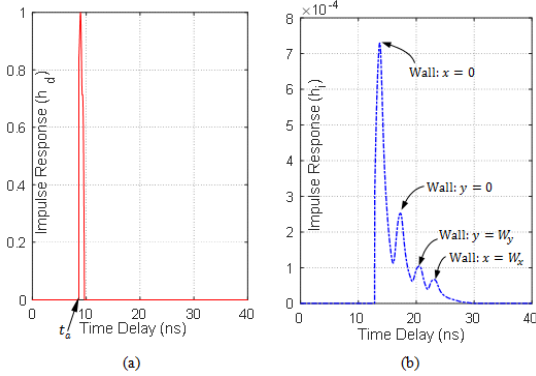
Fig.6: Normalized impulse response at a point $\mathbf{r} = (1\text{m}, 2\text{m}, 1\text{m})$ inside a room of dimensions $5\text{m} \times 5\text{m} \times 3\text{m}$ due to a square LED source of area $45 \text{ cm} \times 45 \text{ cm}$ mounted at the center point of the room ceil , (a) LOS impulse response. (b) Non-LOS impulse response.
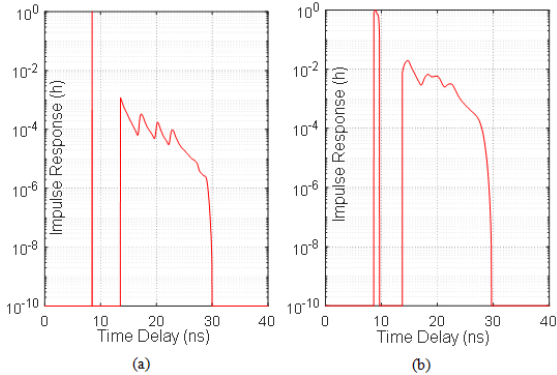
Fig.7: Total (normalized) impulse response at a point $\mathbf{r} = (1\text{m}, 2\text{m}, 1\text{m})$ inside a room of dimensions $5\text{m} \times 5\text{m} \times 3\text{m}$ due to (a) point LED source, (b) square LED source of area $45 \text{ cm} \times 45 \text{ cm}$; the LED source is mounted at the center point of the room ceil.

3.1.2. Received Signal at Arbitrary Point in the Horizontal Plane

It is assumed that the VLC employs intensity modulation using on-off keying (OOK). Also, it is assumed that the LED source transmits the data at a bit rate $R_b = 50$ Mbps.

When a point LED source is used to transmit a pulse that represents a data bit, the pulses that arrive at $\mathbf{r} = (1\text{m}, 2\text{m}, 1\text{m})$ through the LOS and non-LOS are presented in Figures 8a. The total received pulse is presented in Figure 8b in comparison to the

reference pulse. The reference pulse is the pulse that would be received if the impulse response were a pure Dirac-delta function, i.e. the pulse received through the LOS from a point LED source (located at the central point of the actual source). It is shown that the received pulse has two types of distortion; the first type is amplitude distortion due to the addition of the light received through the non-LOS path and the other distortion is caused by the delay-spread due to the delayed light pulse received through the non-LOS path. The power of the ISI is calculated as described in Section 2.5 resulting in SISIR = 15.75 dB.

When a square LED source of area $45 \text{ cm} \times 45 \text{ cm}$ is used to transmit a rectangular pulse of duration $1/R_b$, the received pulses at $\mathbf{r} = (1\text{m}, 2\text{m}, 1\text{m})$ through the LOS and non-LOS are presented in Figures 9a. The total received pulse is shown in Figure 9b in comparison to the reference pulse. As shown in Figure 9b, the received pulse has three types of distortion; the first type caused by the non-zero rising time (slow rising); the second type is amplitude distortion due to the addition of the light received through the non-LOS path; the third type of distortion is caused by the delay-spread due to the spread of both the LOS and non-LOS impulse responses. The power of the ISI is calculated as described in Section 2.5 resulting in SISIR = 12.4 dB. By comparison between Figures 9b and 8b, it is shown that the light pulse received in the case of a square LED source is more distorted than that received in the case of a point LED source and, thereby, resulting in a higher level of ISI.
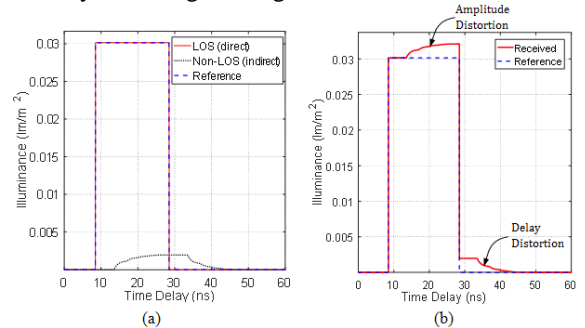
Fig.8: The received optical pulse compared to the reference-received pulse due to a single point LED source at the ceil center in indoor VLC at the point $\mathbf{r} = (1\text{m}, 2\text{m}, 1\text{m})$ in a room of dimensions $5\text{m} \times 5\text{m} \times 3\text{m}$. (a) Components of the received pulse: LOS and non-LOS (b) Total received pulse.

3.2. ISI at the Central Point in Indoor VLC System

It is assumed that the VLC employs intensity modulation using on-off keying (OOK). Also, it is assumed that the LED source transmits the data at a

bit rate $R_b = 50$ Mbps. The LED source is used to transmit a rectangular pulse that represents a data bit. The impulse response, the received pulse, and, hence the ISI are assessed at the center of the horizontal plane of the mobile units ($z = 1$m).

3.2.1. Impulse Response at the Central Point in the Horizontal Plane

Assuming that the mobile unit is at $r = (2.5$m$, 2.5$m$, 1$m$)$ i.e. the center point of the plane $z = z_r$, the impulse response is plotted against the time delay as shown in Figure 10. For a single LED point source at the center of the room ceil, the LOS impulse response is a Dirac-delta function $\delta(t - t_a)$ as shown in Figure 10a. Thus, the LOS impulse response of a VLC channel employing a point LED source is also an impulse at the time of arrival, t_a, that can be calculated using (14) which gives $t_a = 6.7$ ns. On the other hand, the non-LOS impulse response is spread over the time interval $(8 - 26$ ns$)$. However, as shown in Figure 10a, the magnitude of the latter is very low relative to that of the former, the latter is very low relative to the former $(\max(h_i) \sim 10^{-4} \max(h_d))$. Thus, for a point LED source, no spread delay is caused by the LOS illuminance; the spread delay and, hence, the ISI are caused only by the non-LOS illuminance which is very small in comparison to the LOS illuminance.

For a square LED source of area 2.5m $\times 2.5$m mounted on the center of the room ceil, the LOS impulse response is a pulse spread over the interval $(6.7 - 13$ ns$)$ of the delay time as shown in Figure 10b. The non-LOS impulse response is also a pulse spread over the interval $(11 - 37$ ns$)$ of the delay time. Thus, for a square LED source, the spread delay and, hence, the ISI are caused by the LOS as well as the non-LOS illuminance.
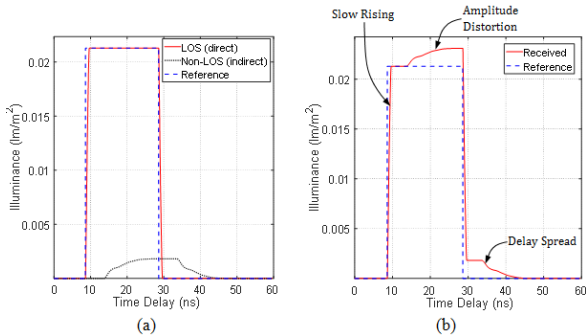
Figure 9: The received optical pulse compared to the reference-received pulse due to a square LED source of area 45 cm $\times 45$ cm mounted at the center point of the room ceil VLC at the point $\mathbf{r} = (1$m$, 2$m$, 1$m$)$ in a room of dimensions 5m $\times 5$m $\times 3$m. (a) Components of the received pulse: LOS and non-LOS (b) Total received pulse.

3.2.2. Received Signal at the Central Point in the Horizontal Plane

When a point LED source is used to transmit a rectangular pulse of duration $\boldsymbol{T_b = 1/R_b}$, the pulse arriving through the LOS and that arriving through the non-LOS at $\mathbf{r_r} = (\mathbf{2.5}m, \mathbf{2.5}m, \mathbf{1}m)$ are shown in Figure 11. The total received pulse is shown in Figure 1b in comparison to the reference pulse. It shown that the received pulse has two types of distortion; the first type is amplitude distortion due to the addition of the light received through the non-LOS path and the other distortion is caused by the delay-spread due to the delayed light pulse received through the non-LOS path. However, the received pulse is weakly distorted and, hence, the resulting SINR is **19.4 dB**.

When a square LED source of area 2.5m $\times 2.5$m mounted at the center of the room ceil is used for transmission, the pulse arriving through the LOS and that arriving through the non-LOS at $\mathbf{r_r} = (2.5$m$, 2.5$m$, 1$m$)$ are shown in Figure 12. The total received pulse is shown in Figure 12b in comparison to the reference pulse. As shown in Figure 12b, the received pulse has three types of distortion; the first type caused by the non-zero rising time (slow rising); the second type is amplitude distortion due to the addition of the light received through the non-LOS path; the third type of distortion is caused by the delay-spread due to the spread of both the LOS and non-LOS impulse responses. The received pulse is significantly distorted and the resulting SINR is 8.6 dB.
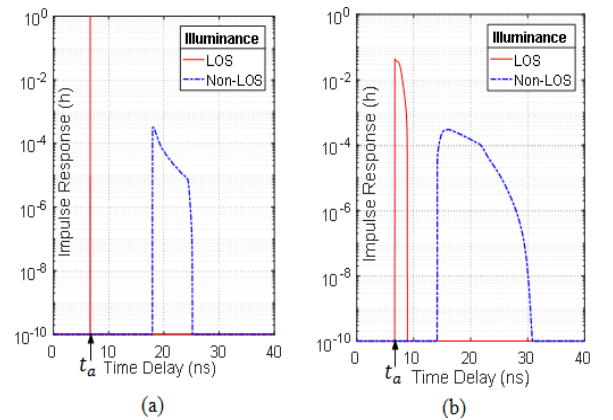
Fig.10: Normalized impulse response due to direct (LOS) propagation and indirect (non-LOS) propagation in indoor VLC at the point $(2.5$m$, 2.5$m$, 1.0$m$)$ in a room of dimensions 5m $\times 5$m $\times 3$m. (a) Point LED source at the ceil center. (b) Square LED source of area $(2.5$m $\times 2.5$m$)$ at the ceil center.
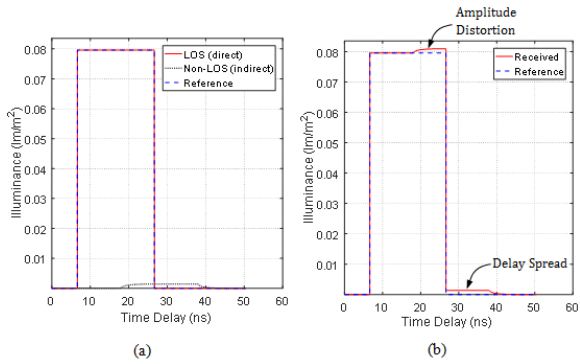
Fig.11: The received optical pulse compared to the reference-received pulse due to a single LED point source at the ceil center in indoor VLC at the point $(2.5m, 2.5m, 1.0m)$ in a room of dimensions $5m \times 5m \times 3m$. (a) Components of the received pulse: LOS and non-LOS (b) Total received pulse.
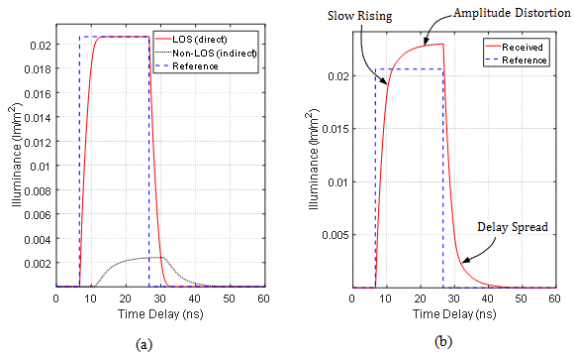
Fig.12: The received optical pulse compared to the reference-received pulse due to a LED source of square area $(2.5m \times 2.5m)$ at the center of the ceil in indoor VLC system at the point $(2.5m, 2.5m, 1.0m)$ in a room of dimensions $5m \times 5m \times 3m$. (a) Components of the received pulse: LOS and non-LOS (b) Total received pulse.

3.3. Dependence of the Impulse Response on the Area of the LED Source

The impulse response of the VLC channel when the receiver location is $r = (2.5m, 2.5m, 1m)$ is presented in Figure 13a, the LOS impulse response is a spread pulse whose width increases with increasing the area of the LED source. As the receiver is at the center of the horizontal room, the start time of the LOS impulse response, as shown in Figure 13a, is independent of the LED source area. As shown in Figure 13b, the non-LOS impulse response is a spread pulse of low level magnitude relative to that of the LOS impulse response. It is shown that both the magnitude and width of the pulse representing the non-LOS impulse response increase with increasing the area of the LED source.
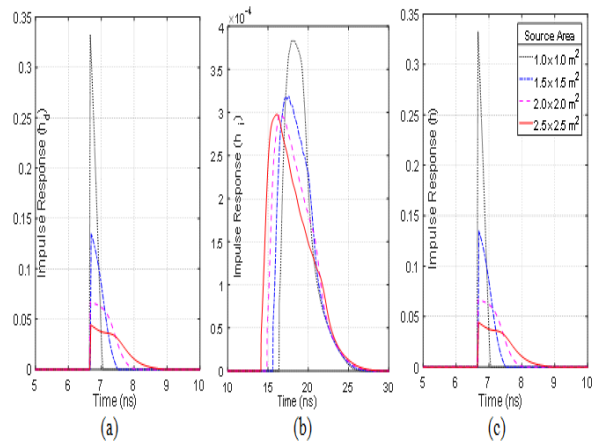
Fig.13: Impulse response due to a square LED source of different areas mounted at the center of the room ceil in indoor VLC system inside a room of dimensions $5m \times 5m \times 3m$ when the receiver location is $r = (2.5m, 2.5m, 1m)$. (a) LOS impulse response. (b) Non-LOS impulse response. (c) Total impulse response.

The received pulse at the location $\mathbf{r_r} = (2.5m, 2.5m, 1m)$ and its LOS and non-LOS components when a rectangular pulse of duration $T_b = 1/R_b$ is transmitted by a square LED source of different areas (mounted at the center of the room ceil) are shown in Figure 14. The light propagation is performed in indoor VLC channel inside a room of dimensions $5m \times 5m \times 3m$. As shown in Figure 14a, the amplitude of the pulse received through LOS propagation decreases with increasing the area of the LED source. In contrary, the pulse received through non-LOS propagation increases with increasing the LED source area. The total received pulse is presented in Figure 14c in comparison to the receiver reference for each case.
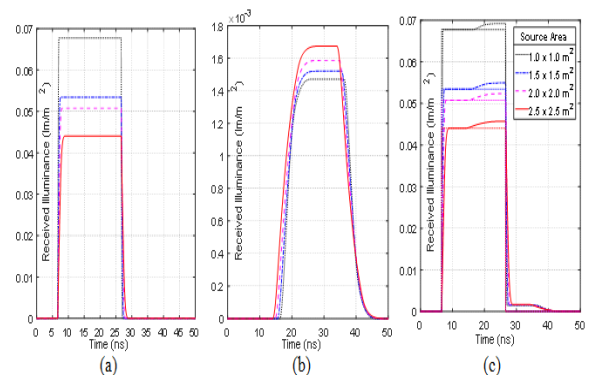
Fig.14: Received pulse due to a square LED source of different areas mounted at the center of the room ceil when the receiver location is $r = (2.5m, 2.5m, 1m)$ in indoor VLC system inside a room of dimensions $5m \times 5m \times 3m$. (a) Received pulse through LOS propagation. (b) Received pulse through non-LOS propagation. (c) Total received pulse.

When the light propagation is impaired only by the ISI caused by the delay spread, the dependencies of the average propagation delay, RMS delay spread, and SINR on the width of the LED source are shown in Figures 15a, 15b, and 15c, respectively. It is shown that increasing the area of the LED source has effect of increasing the RMS delay spread and, hence, decreasing the SINR. It is shown that, as the mobile unit is moving towards the room center, the average propagation delay and RMS delay spread are decreased and the resulting SINR is increased. As the mobile unit is moving towards the room corner, the average propagation delay and RMS delay spread are increased and the resulting SINR is decreased.
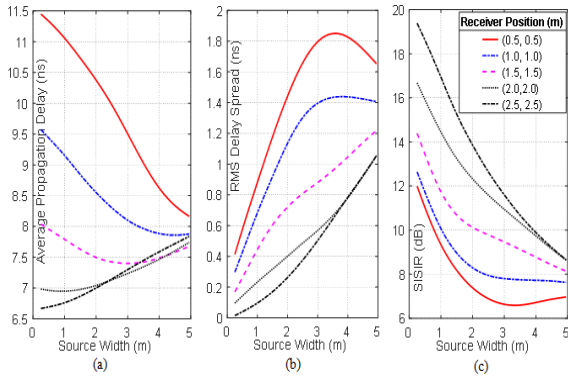
Fig.15: Dependence of the ISI on the width of the LED source for receivers at different positions (a) Average propagation delay. (b) RMS delay spread. (c) SISIR.

3.4. Noise and Ambient Light Impairing Indoor Light Propagation

In the present analysis, as explained in Section 2.3, it is assumed that the noise resulting from the thermal noise, shot noise and ambient light can be modelled as AWGN. Also, at the different locations over the plane of the mobile receivers, the power of the AWGN is assumed to have random distribution with a given variance and correlation length and Gaussian correlation function. For complete representation of the typical noise existing in indoor VLC, the distribution of the AGWN shown in Figure 16 is generated assuming that the noise variance is $\sigma_n^2 = 5 \times 10^{-2}$ and the correlation function is Gaussian with correlation length of **2.5m**.

3.5. Distribution of Illumination on the Horizontal Plane

The distribution of the received signal (illuminance) in the plane of the mobile units ($z = 1m$) is presented in Figure 17 when the light propagation is neither impaired by ISI nor ambient light in a VLC

system inside a room of dimensions **5m × 5m × 3m**. The illuminance distribution is presented for two types of light sources: a point LED source and a squared LED source of area **1m × 1m**. It should be noted that the light source is mounted on the room ceil at its center point and the mobile receiving photodetectors are assumed to have **FOV = 90°** and responsivity **$\eta = 1$**. It is clear that the illumination of the horizontal plane obtained in the case of using a point LED source is relatively higher than that obtained in the case of the 1m × 1m square LED source.
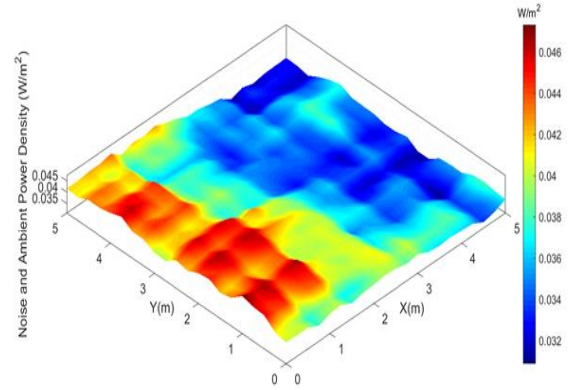
Fig.16: Distribution of the ambient light (power density) over the plane of the mobile receivers ($z = 1m$), $\sigma_n^2 = 5 \times 10^{-2}$, in a VLC system inside a room of dimensions 5m × 5m × 3m.

3.6. Distribution of the ISI in the Horizontal Plane

The distribution of the SISIR in the plane of the mobile units ($z = 1m$) is presented in Figure 18 for a VLC system inside a room of dimensions 5m × 5m × 3m. The distribution of the SINR is presented for two types of light sources: a point LED source and a squared LED source of area 1m × 1m. It should be noted that the light source is mounted on the room ceil at its center point and the mobile receiving photodetectors are assumed to have FOV = 90° and responsivity $\eta = 1$. It is clear that the SISIR of the horizontal plane obtained in the case of using a point LED source is significantly higher than that obtained in the case of the 1m × 1m square LED source.

3.7. Distribution of the SISIR in the Horizontal Plane

The signal-to-ISI ratio (SISIR) is the SINR when the light propagation is impaired only by ISI, i.e. under the assumption that $\sigma_n^2 = 0$. The distribution of the SISIR in the plane of the mobile units ($z = 1m$) is presented in Figure 19 for a VLC system inside a

room of dimensions $5m \times 5m \times 3m$. The distribution of the SINR is presented for two types of light sources: a point LED source and a squared LED source of area $1m \times 1m$. It should be noted that the light source is mounted on the room ceil at its center point and the mobile receiving photodetectors are assumed to have FOV = 90° and responsivity $\eta = 1$. It is clear that the SISIR of the horizontal plane obtained in the case of using a point LED source is significantly higher than that obtained in the case of the $1m \times 1m$ square LED source.

3.8. Distribution of the SINR in the Horizontal Plane

The SINR when the light propagation is impaired only by ISI and AWGN under the assumption that $\sigma_n^2 = 5 \times 10^{-2}$ in the plane of the mobile units $(z = 1m)$ is presented in Figure 20 for a VLC system inside a room of dimensions $5m \times 5m \times 3m$. The distribution of the SINR is presented for two types of light sources: a point LED source and a squared LED source of area $\mathbf{1m \times 1m}$. It should be noted that the light source is mounted on the room ceil at its center point and the mobile receiving photodetectors are assumed to have $\mathbf{FOV = 90°}$ and responsivity $\boldsymbol{\eta = 1}$. It is shown that the SINR of the horizontal plane obtained in the case of using a point LED source is higher than that obtained in the case of the $\mathbf{1m \times 1m}$ square LED source. In both cases, the SINR is maximum in the room center and minimum in the regions near the room corners.

3.9. Distribution of the BER in the Horizontal Plane

The distribution of the BER over the horizontal area of the mobile units is presented in Figure 21 for a white LED source of area $1m \times 1m$ mounted at the center of the room ceil. It is shown that the BER have its maximum values at the room corners which do not exceed 5×10^{-5}.

3.10. Effect of the Radiated Light Power on the VLC System Performance

As shown in Figure 21, the worst BER is 5×10^{-5} and is found at the room corner for radiated light power of $P_{Tx} = 10\ W$. Increasing the radiated power leads to improve the worst BER as shown in Figure 22. For $P_{Tx} = 50\ W$, the worst value of the BER is improved to be 3×10^{-6}.

4. Conclusion

A detailed method is introduced for the assessment of the ISI encountered in indoor VLC system inside a room of area $\leq 5m \times 5m$. The SISIR is evaluated over the horizontal plane of the mobile units. A comparative performance assessment between the VLC system employing a point LED source and that employing a light source of rectangular area is presented. The overall environmental noise impairing the indoor light propagation is modelled as additive white Gaussian noise (AWGN). The SINR including the effects of ISI and AWGN is evaluated over the horizontal plane of the mobile units. The dependencies of the average propagation delay, RMS delay spread, and SINR on the area of the LED source are studied. It is shown the SISIR for the indoor VLC system under consideration is degraded with increasing the area of the LED source. Also, it is shown that for relatively low level of the AWGN, that the performance of the indoor VLC is significantly degraded with increasing the area of the LED source.
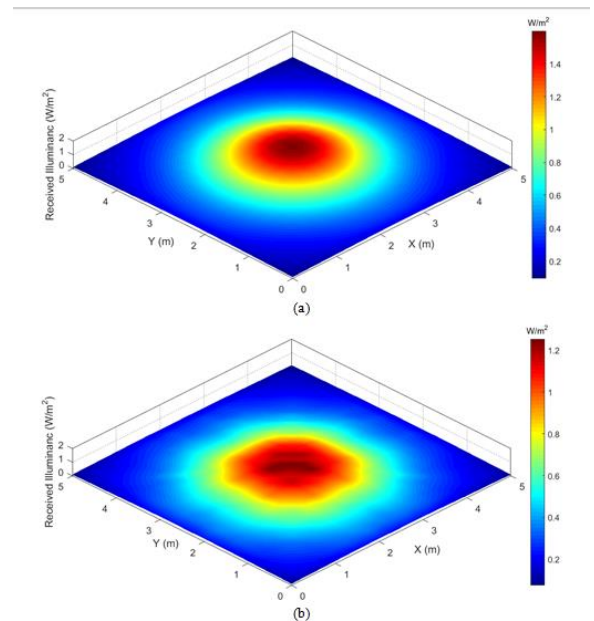
Fig.17: Distribution of the received signal (illuminance) in the plane of the mobile receivers (z = 1m) when the light propagation is neither impaired by ISI nor ambient light in a VLC system inside a room of dimensions $5m \times 5m \times 3m$; the light source is mounted on the room ceil at its center point; the mobile receivers have FOV = 90°; the VLC system employs (a) point LED source, (b) square LED source of area 1m × 1m.
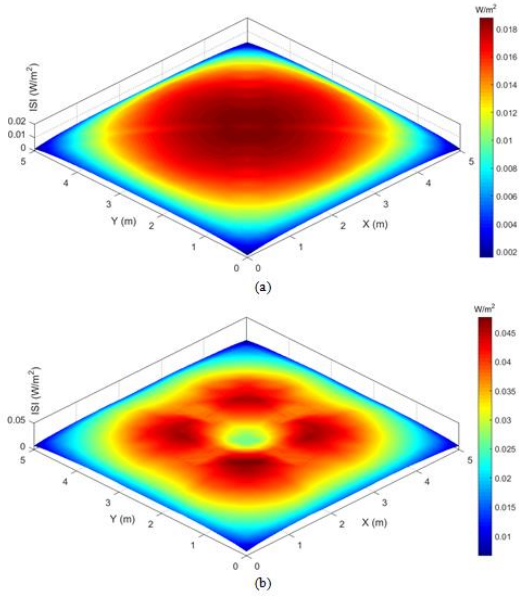
Fig.18: Distribution of the illuminance caused by ISI in the plane of the mobile units ($z = 1m$) in VLC system inside a room of dimensions $5m \times 5m \times 3m$; the light source is mounted on the room ceil at its center point; the mobile receivers have FOV $= 90°$; the VLC system employs (a) point LED source, (b) square LED source of area $1m \times 1m$.
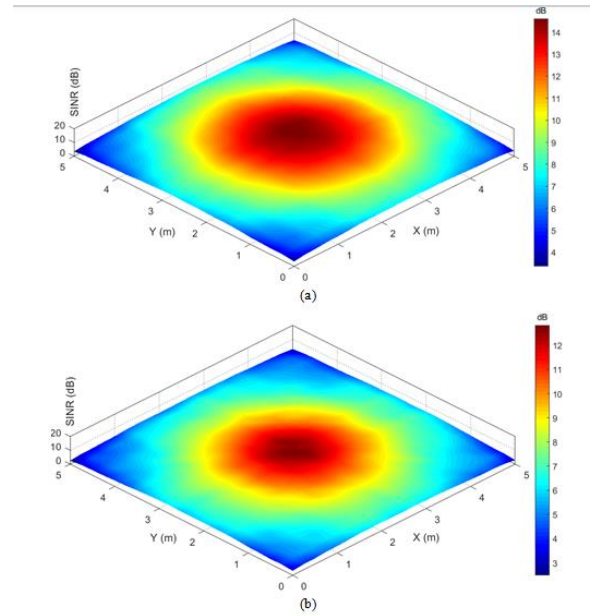
Fig.20: Distribution of the SINR in the plane of the mobile receivers ($z = 1m$) when the indoor light propagation is impaired by both ISI and AWGN with $\sigma_n^2 = 5 \times 10^{-2}$ in a VLC system inside a room of dimensions $5m \times 5m \times 3m$; the light source is mounted on the room ceil at its center point; the mobile receivers have FOV $= 90°$; the VLC system employs (a) point LED source, (b) square LED source of area $1m \times 1m$.

Fig.21: Distribution of the BER in the plane of the mobile receivers ($z = 1m$) when the indoor light propagation is impaired by both ISI and AWGN with $\sigma_n^2 = 5 \times 10^{-2}$ in a VLC system inside a room of dimensions $5m \times 5m \times 3m$; the light source is mounted on the room ceil at its center point; the mobile receivers have FOV $= 90°$; the VLC system employs a square LED source of area $1m \times 1m$.
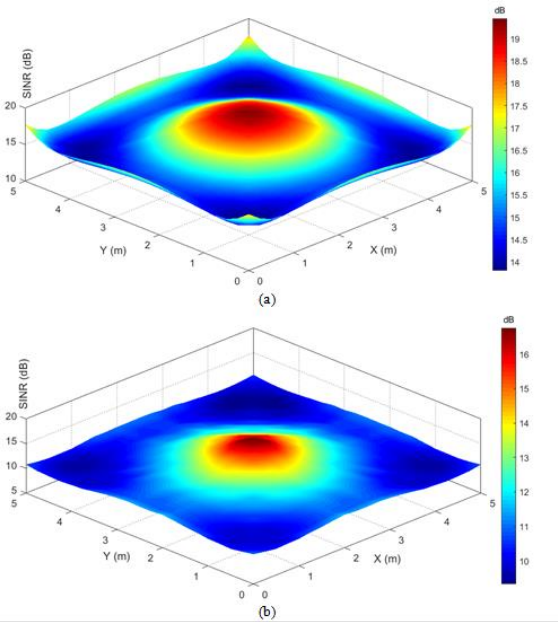
Fig.19: Distribution of the SISIR in the plane of the mobile units ($z = 1m$) when the light propagation is impaired only by ISI in VLC system inside a room of dimensions $5m \times 5m \times 3m$; the light source is mounted on the room ceil at its center point; the mobile receivers have FOV $= 90°$; the VLC system employs (a) point LED source, (b) square LED source of area $1m \times 1m$.

73
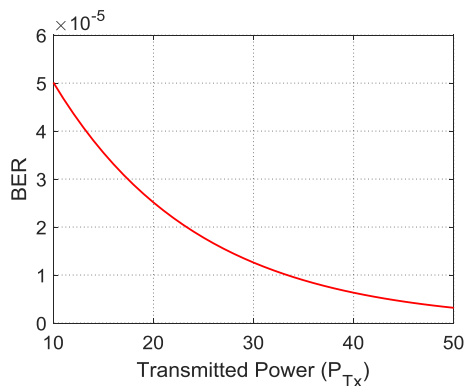
Fig.22: Dependence of the BER at the room corner in the plane of the mobile receivers $(z = 1m)$ on the radiated light power, P_{Tx}, when the indoor light propagation is impaired by both ISI and AWGN with $\sigma_n^2 = 5 \times 10^{-2}$ in a VLC system inside a room of dimensions $5m \times 5m \times 3m$; the light source is mounted on the room ceil at its center point; the mobile receivers have FOV = 90°; the VLC system employs a square LED source of area $1m \times 1m$.

References

[1] K. Shaaban, M. H. M. Shamim, & K. Abdur-Rouf, (2021), "Visible light communication for intelligent transportation systems: A review of the latest technologies", Journal of Traffic and Transportation Engineering (English Edition), 8(4), 483–492. doi:10.1016/j.jtte.2021.04.005.

[2] A. Singh, G. Ghatak, A.Srivastava, V. A. Bohara, & A. K. Jagadeesan, (2021), "Performance Analysis of Indoor Communication System Using Off-the-Shelf LEDs with Human Blockages", IEEE Open Journal of the Communications Society, 2, 187–198. doi:10.1109/ojcoms.2020.3048954 .

[3] N.Chaudhary, O. I. Younus, L. N .Alves, Z.Ghassemlooy, S. Zvanovec , & H. Le-Minh, (2021), "An Indoor Visible Light Positioning System Using Tilted LEDs with High Accuracy", Sensors, 21(3), 920. doi:10.3390/s21030920.

[4] Y. Chen, S. Li, and H. Liu, "Dynamic frequency reuse based on improved tabu search in multi-user visible light communication networks", *IEEE Access* 7 (2019): 35173-35183.

[5] I. Abdalla, M.B. Rahaim, and T.D.C. Little, "Interference in multi-user optical wireless communications systems", *Philosophical Transactions of the Royal Society A* 378.2169 (2020): 20190190.

[6] M.W. Eltokhey, M.A. Khalighi, and Z.Ghassemlooy, "Multiple access techniques for VLC in large space indoor scenarios: A comparative study", *2019 15th International Conference on Telecommunications (ConTEL)*. IEEE, 2019

[7] C. Chen, N.Serafimovski, and H. Haas, "Fractional frequency reuse in optical wireless cellular networks", 2013 *IEEE* 24th *annual international symposium on personal, indoor, and mobile radio communications (PIMRC)*. IEEE, 2013.

[8] J. Lian, Z. Vatansever, & M. Noshad, "Indoor visible light communications, networking, and

[9] applications", *Journal of Physics: Photonics* 1.1 (2019): 012001.

[9] D. De-qiang, and K. Xi-zheng ,"A new indoor VLC channel model based on reflection", *Optoelectronics Letters* 6.4 (2010): 295-298.

[10] K. Lee, H. Park, and J. R. Barry,"Indoor channel characteristics for visible light communications." *IEEE communications letters* 15.2 (2011): 217-219.

[11] Y. Qiu, H. Chen, and W. Meng, "Channel modeling for visible light communications—a survey", *Wireless Communications and Mobile Computing* 16.14 (2016): 2016-2034.

[12] Z. Ghassemlooy, L.N. Alves, S. Zvanovec, "*Visible light communications: theory and applications"*, CRC press, 2017.

[13] A.A.A. Al-Kinani, "*Channel modelling for visible light communication systems*", Diss. Heriot-Watt University, 2018.

[14] A. M. Ramirez-Aguilera, J.M. Luna-Rivera, & J. Rabadan, "A review of indoor channel modeling techniques for visible light communications". *2018 IEEE 10th Latin-American Conference on Communications (LATINCOM)*. IEEE, 2018.

[15] K. Lee, H. Park, and J. R. Barry, "Indoor channel characteristics for visible light communications", IEEE Communications Letters, Vol. 15, No. 2, pp.217-219, 2011.

[16] K. Lee and H. Park, "Channel model and modulation schemes for visible light communications", In 2011 IEEE 54th International Midwest Symposium on Circuits and Systems (MWSCAS), pp. 1-4, August, 2011.

[17] T. Komine ,and M. Nakagawa, "Fundamental analysis for visible-light communication system using LED lights", IEEE transactions on Consumer Electronics Vol. 50, No. 1, pp. 100-107, 2004.

[18] H. H. Qamar, K. F. A. Hussein, and M. B. El-Mashade, "Assessment of signal strength in indoor optical wireless communications using diffuse infrared radiation", In 2019 36th National Radio Science Conference (NRSC), pp. 108-117, IEEE, 2019.

[19] H. H. Qamar, A. E. Farahat, K. F. A. Hussein, and M. B. El Mashade, "Assessment of scattering of plane waves on optically illuminated area of rough surface", Progress In Electromagnetics Research, Vol. 86, pp. 77-102, 2020.

[20] H. H. Qamar, M. B. El-Mashade, A. E. Farahat, and K. F. A Hussein, "Convergence of ensemble averaging for optical scattering on rough surfaces using GTD-RT", In 2019 6th International Conference on Advanced Control Circuits and Systems (ACCS) & 2019 5th International Conference on New Paradigms in Electronics & information Technology (PEIT), pp. 167-175, IEEE, 2019.

[21] S. A. M, Soliman, A. E. Farahat, K. F. A. Hussein, and A.E. A. Ammar, "Spatial Domain Generation of Random Surface Using Savitzky-Golay Filter for Simulation of Electromagnetic Polarimetric Systems", Applied Computational Electromagnetics Society Journal Vol. 34, No. 1, 2019.